22. C. Vance *et al.*, *Brain* **129**, 868 (2006).
23. D. M. Ruddy *et al.*, *Am. J. Hum. Genet.* **73**, 390 (2003).
24. W. J. Law, K. L. Cann, G. G. Hicks, *Brief. Funct. Genomics Proteomics* **5**, 8 (2006).
25. Y. Kanai, N. Dohmae, N. Hirokawa, *Neuron* **43**, 513 (2004).
26. A. Yoshimura *et al.*, *Curr. Biol.* **16**, 2345 (2006).
27. K. J. De Vos, A. J. Grierson, S. Ackerley, C. C. Miller, *Annu. Rev. Neurosci.* **31**, 151 (2008).
28. This publication is dedicated to the patients and families who have contributed to this project and to B. Coote and C. Cecere for blood sample collection. Postmortem tissues were provided by MRC Neurodegenerative Diseases Brain Bank. This work was supported in the United Kingdom by grants from the American ALS Association, the Middlemass family, Lady Edith Wolfson Trust, Motor Neurone Disease Association UK, The Wellcome Trust, European Union (APOPIS consortium, contract LSHM-CT-2003-503330, and NeuroNE Consortium), National Institute for Health Research Biomedical Research Centre for Mental Health, The South London and Maudsley National Health Service Foundation Trust, Medical Research Council UK, a Jack Cigman grant from King's College Hospital Charity, The Heaton-Ellis Trust, and The Psychiatry Research Trust of the Institute of Psychiatry. In Australia the work was supported by the Australian National Health and Medical Research Council (CDA 511941) and a Peter Stearne grant from the Motor Neuron Disease Research Institute of Australia.

Supporting Online Material

www.sciencemag.org/cgi/content/full/323/5918/1208/DC1
Materials and Methods
Figs. S1 and S2
Tables S1 to S4
References

15 September 2008; accepted 16 December 2008
10.1126/science.1165942

Synchronous Hyperactivity and Intercellular Calcium Waves in Astrocytes in Alzheimer Mice

Kishore V. Kuchibhotla,[1,2] Carli R. Lattarulo,[1] Bradley T. Hyman,[1] Brian J. Bacskai[1]*

Although senile plaques focally disrupt neuronal health, the functional response of astrocytes to Alzheimer's disease pathology is unknown. Using multiphoton fluorescence lifetime imaging microscopy in vivo, we quantitatively imaged astrocytic calcium homeostasis in a mouse model of Alzheimer's disease. Resting calcium was globally elevated in the astrocytic network, but was independent of proximity to individual plaques. Time-lapse imaging revealed that calcium transients in astrocytes were more frequent, synchronously coordinated across long distances, and uncoupled from neuronal activity. Furthermore, rare intercellular calcium waves were observed, but only in mice with amyloid-β plaques, originating near plaques and spreading radially at least 200 micrometers. Thus, although neurotoxicity is observed near amyloid-β deposits, there exists a more general astrocyte-based network response to focal pathology.

Growing evidence supports the hypothesis that in Alzheimer's disease (AD), synapses fail and dendritic spines are lost in the amyloid-β (Aβ) plaque microenvironment through a combination of changes in synaptic drive, calcium overload, and the activation of calcium-dependent degenerative processes (*1*–*4*). Neurons, however, make up only part of the brain's volume, with astrocytes making up the bulk of the remainder. Astrocytes form a structurally interconnected network that, in vitro, exhibit distinct long-distance signaling properties that might be revealed in vivo only after pathological trauma. The idea that neural network dysfunction and degeneration also fully mediate the memory loss in AD does not reflect the growing in vivo evidence that astrocytes play an important role in cortical circuit function (*5*–*7*). In AD, pathological studies of human cases and mouse models have shown that astrocytes surround plaques and might play a critical role in Aβ deposition and clearance (*8*–*10*). Given the profound impact of Aβ deposition on nearby neuronal calcium homeostasis and synaptic function, it is reasonable to hypothesize that astrocyte networks would also be perturbed and might contribute to cortical dysfunction (*11*). We sought to test whether senile plaque deposition would similarly affect astrocyte calcium homeostasis or dynamic signaling in vivo in a mouse model of AD.

To answer these questions, we used multiphoton fluorescent lifetime imaging microscopy (FLIM) to measure resting calcium levels in astrocytes of live mice with cortical plaques (*12*). We multiplexed the fluorescent properties of a small-molecule calcium dye [Oregon-Green BAPTA-1 (OGB)] in the same experimental model and for the same group of cells (Fig. 1A); we used OGB both as a relative indicator of astrocytic activity (intensity) and as a quantitative measure of steady-state intracellular calcium concentration ([Ca]i) (lifetime). We used mice that express mutant human Aβ precursor protein (APP) and mutant presenilin 1 (PS1) (APPswe:PS1ΔE9) in neurons. These mutations lead to an increase in Aβ production and plaque deposition beginning at ~4.5 months of age (*13*, *14*). In mice with plaques, resting [Ca]i in astrocytes was higher than in wild-type animals (Fig. 1, B to F). The resting [Ca]i of astrocytes in wild-type mice was 81 ± 3 nM, whereas in transgenic mice the resting [Ca]i was 149 ± 6 nM ($P < 0.05$). We confirmed that the surrounding neuropil signal minimally contaminated the astrocyte [Ca]i (fig. S2). We next mapped the spatial distribution of astrocytes versus Aβ plaque location in three dimensions (fig. S3). There was no effect of plaque proximity on resting [Ca]i in individual astrocytes (Fig. 1G; $n > 25$ cells per bin). However, plaques deposit rapidly in these mice, so that very few astrocytes were farther than 100 μm away from a plaque.

Using time-lapse calcium imaging of OGB intensity, we measured spontaneous astrocytic activity. Astrocytes in adult APP/PS1 mice (6 to 8 months old) with cortical plaques exhibited a significant increase in spontaneous activity (Fig. 2 and movies S1 and S2). 27.9 ± 6.0% of all astrocytes were active in APP/PS1 mice when compared with the relatively rare spontaneous events seen in wild-type mice (8.1 ± 2.3%; $P < 0.05$) (Fig. 2B). APP/PS1 mutant mice did not show evidence of altered spontaneous activity before they developed senile plaques (at 3 to 3.5 months old) (Fig. 2B). Furthermore, the amplitude $\Delta F/F$ of the calcium signals was significantly higher in APP/PS1 mice ($\Delta F/F$, 33.6 ± 1.1%) when compared with that of wild-type mice ($\Delta F/F$, 23.2 ± 0.8%, $P < 0.001$) (fig. S4). This change in astrocytic function was also independent of plaque proximity (Fig. 2C and fig. S4), again implicating a global astrocytic response to plaque deposition. It was possible that our measurements of baseline resting calcium using FLIM (Fig. 1) reflected this increased astrocyte spontaneous activity rather than a change in baseline resting calcium. To test this, we coregistered FLIM data with spontaneous activity data to allow single-cell identification across imaging modalities. Spontaneously active cells did not have significantly different resting calcium than non-active cells (Fig. 1H, $P = 0.811$).

In this mouse model, astrocytes do not produce Aβ, which suggests a non–cell-autonomous mechanism behind the increased activity. Hyperactive neurons in the plaque penumbra (*2*) might be responsible by inducing increased activity in functionally connected astrocytes. To test this, we blocked neuronal activity with the sodium-channel blocker tetrodotoxin (TTX) (Fig. 2, D to F, and fig. S5). Under these conditions, astrocytic activity persisted (Fig. 2F). Thus, the increase in astrocyte activity does not derive from neuronal hyperactivity near Aβ deposits, which supports the hypothesis that Aβ interacts directly with the astrocyte network.

Astrocytes play a local role in supporting neuronal activity and in mirroring neuronal responses

[1]Massachusetts General Hospital, Department of Neurology/Alzheimer's Disease Research Laboratory, 114 16th Street, Charlestown, MA 02129, USA. [2]Program in Biophysics, Harvard University, Cambridge, MA 02138, USA.

*To whom correspondence should be addressed. E-mail: bbacskai@partners.org

to sensory stimuli (*6*). There is little in vivo evidence supporting the hypothesis that astrocytes form long-range signaling networks (*7*, *15*). To test this in the AD mouse model, we measured the correlation in activity for all active astrocyte cell pairs in a given imaging field. Two cells that were synchronously active would have a robust central peak in the cross-correlogram. There was a sizable increase in the central peak of the correlogram for the transgenic astrocyte cell pairs (Fig. 3A and fig. S6).

We next compared the average correlation coefficient as a function of the pairwise distance of the two cells (Fig. 3B) and modeled the relationship with distance as an exponential function. In wild-type mice, activity was correlated only when cells were within 50 μm of each other ($P < 0.05$, Kruskal-Wallis with Tukey-Kramer post hoc test). In transgenic mice, there was increased correlated activity as compared with that of the wild type ($P < 0.001$, Mann-Whitney U test) that persisted at distances beyond 50 μm ($P < 0.01$, Kruskal-Wallis with Tukey-Kramer post hoc test). Even at cell-to-cell distances of up to 200 μm, there was a significant elevation in correlated activity as compared with that of the wild type. This can be further seen when comparing the exponential fits: the decay constant was 2.4 times longer in transgenic (–0.020) than in wild-type (–0.008) mice.

Thus, astrocytes in mice with cortical plaques exhibit functional coordination of their intracellular calcium signals at long distances. Indeed, we observed intercellular calcium waves (ICWs) in six out of eight transgenic mice but never in wild-type mice (Fig. 4; $n = 8$ transgenic and 5 nontransgenic mice; $P < 0.05$, Fisher exact test). These waves traveled 196 ± 41 μm at a speed of 22.7 ± 6.4 μm/s, similar to that observed in cells

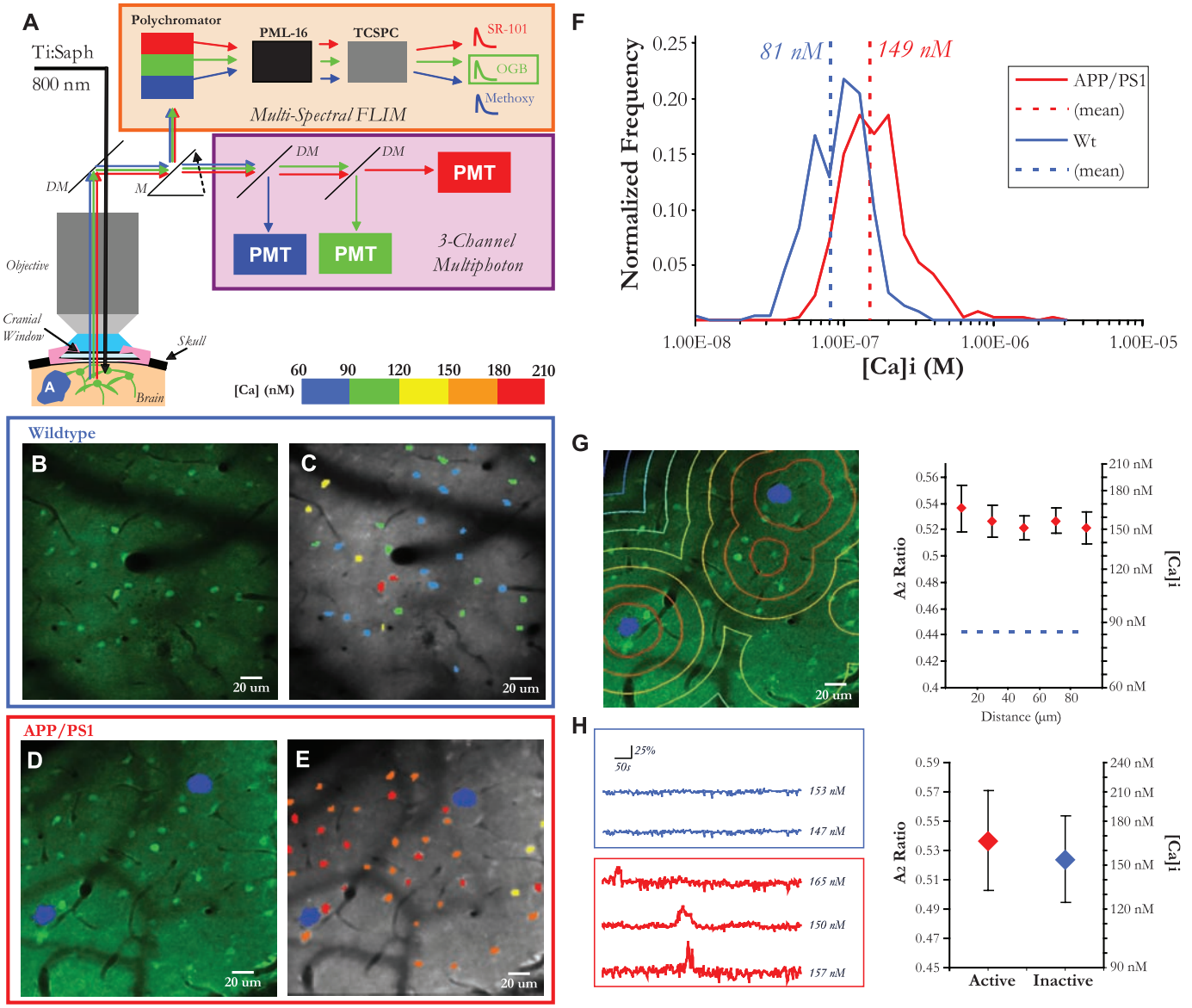

Fig. 1. Resting calcium is globally elevated in astrocytic networks. (**A**) Multiphoton laser illumination simultaneously excited methoxy-XO4 (blue, Aβ), OGB (green, neurons and astrocytes), and SR-101 (red, astrocytes) through a cranial window. The resulting fluorescence emission was sent to either (*1*) a three-channel intensity-based photomultiplier tube (PMT) module or (*2*) a 16-channel multispectral FLIM detector. A single-photon counter (TCSPC) recorded fluorescence lifetime data. (**B** to **E**) Fluorescence decay curves were fit with a calcium-bound lifetime (2359 ps) and an unbound calcium lifetime (569 ps) for each pixel. The pixel data were averaged to obtain single-cell calcium levels, depicted with a calibrated color bar [(C) and (E)]. (**F**) Astrocytes in APP/PS1 mice with cortical plaques [(D) and (E), blue] exhibited significantly higher levels of [Ca]i than those in wild-type mice [(B) and (C)] {$P < 0.05$, Student's t test, $n = 241$ cells in 3 mice [wild type (Wt)], $n = 364$ cells in 3 mice [transgenic (Tg)]}. (**G**) Astrocyte resting [Ca]i did not depend on proximity to a plaque ($P = 0.9194$, Kruskal-Wallis test, $n > 25$ cells for each distance group). (**H**) There was no difference in resting calcium between cells that were active versus inactive ($P = 0.811$, Student's t test, $n = 209$ cells in three mice).

in culture (*16*). The "initiator" astrocyte was located 24.8 ± 7.8 μm from the nearest senile plaque, a proximity that has been previously associated with increased synapto- and neurotoxicity (*3*, *4*). This was significantly closer than the average distance of an astrocyte to the nearest plaque (Fig. 4D; active = 52.5 ± 2.3 μm, inactive = 52.3 ± 1.2 μm, $P < 0.05$). Calcium transients during an ICW ($\Delta F/F$, 45.2 ± 2.4%) were higher in magnitude than a typical spontaneous event in transgenic mice (Fig. 4E; $\Delta F/F$, 30.1 ± 1.5%, $P < 0.01$), suggesting that this signal was different from that spread by nonwave activity.

Astrocytes, in normal conditions, can have highly localized and independent responses (*6*).

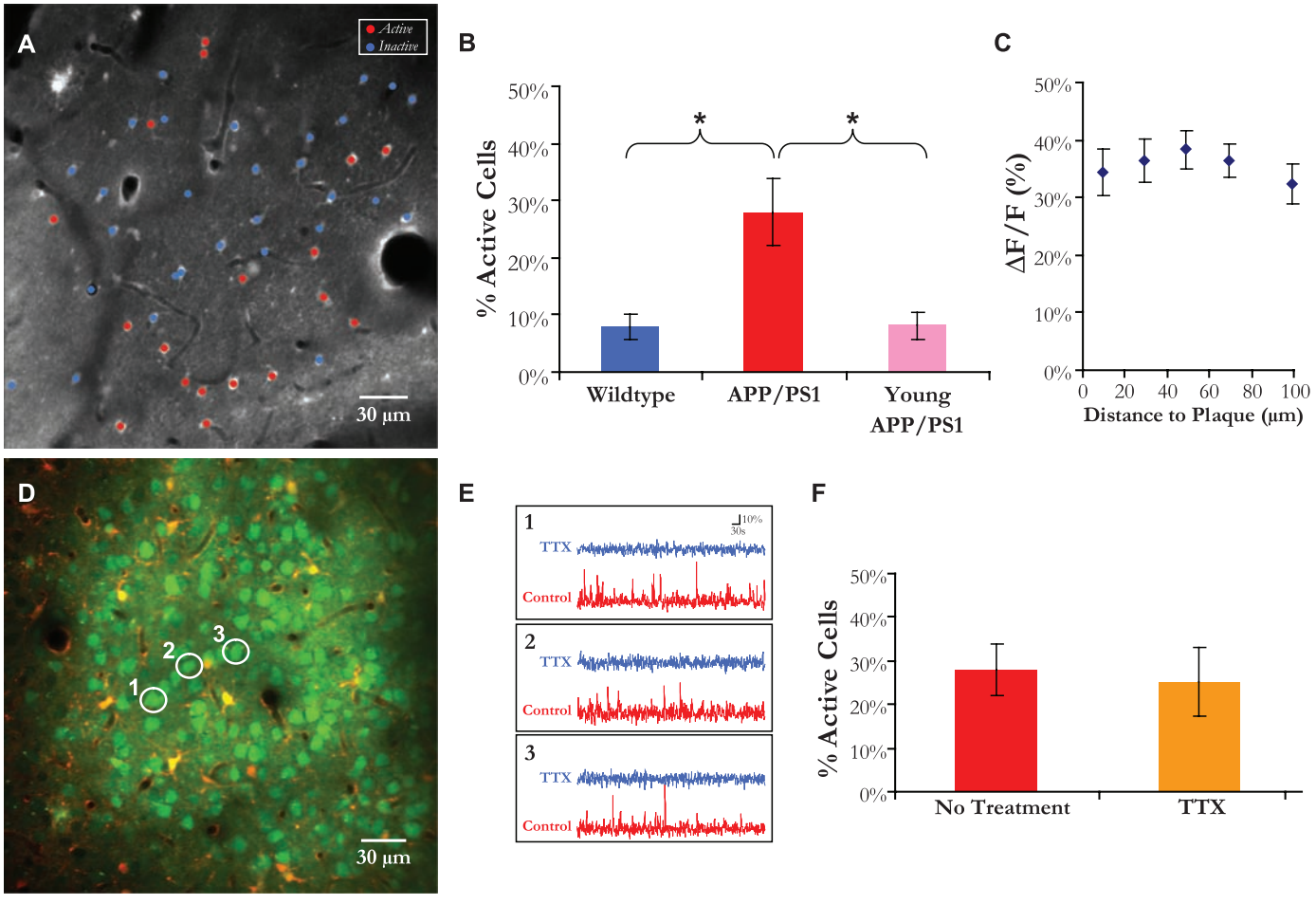

Fig. 2. Neuron-independent increase in spontaneous activity throughout the astrocytic network. (**A**) Cell-activity map overlaid on a multiphoton image of astrocytes. (**B**) There were more spontaneously active cells in mice with cortical plaques (*$P < 0.05$, Kruskal-Wallis with Tukey-Kramer post hoc test, $n = 15$ mice: 8 APP/PS1 with plaques, 4 nontransgenic; and 3 APP/PS1 before plaque deposition). (**C**) The amplitude of the [Ca]i transients ($n = 160$ astrocytes) did not depend on proximity to plaques ($P = 0.9178$, Kruskal-Wallis test). (**D**) Multiphoton image of neurons and astrocytes in an APP/PS1 transgenic mouse with cortical plaques. Three neurons are highlighted to show their spontaneous activity traces before and after application of 1 μM TTX in (**E**). (**F**) There was no reduction in the percentage of active astrocytes in the presence of TTX [27.9 ± 6.0% in control ($n = 8$ mice, 1241 astrocytes) versus 25.4 ± 7.8% under TTX ($n = 4$ mice, 818 astrocytes), $P = 0.8081$, Mann-Whitney U test].

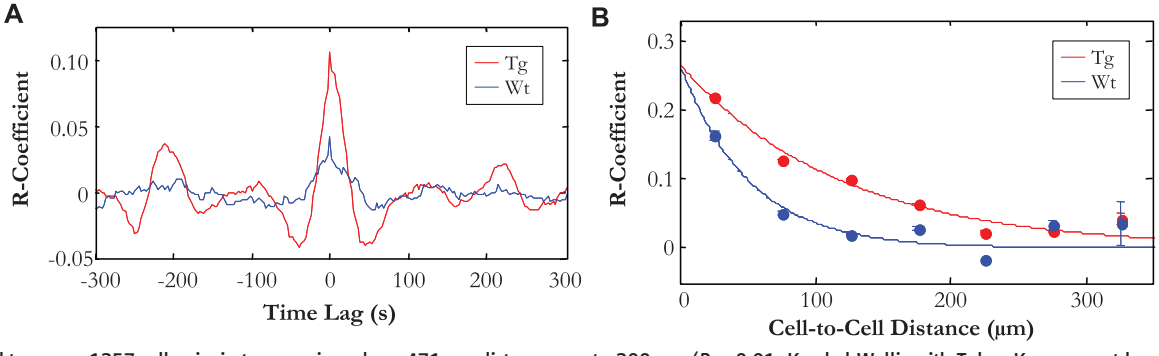

Fig. 3. Spatiotemporal synchrony of astrocytic calcium signaling in APP/PS1 mice. (**A**) The mean cross-correlogram for all active cell pairs (excluding autocorrelations) in transgenic and nontransgenic mice. In APP/PS1 mice there was an increase in the probability that two cells had coordinated activity ($n =$ 3 mice for APP/PS1 and wild type, $n = 1257$ cell pairs in transgenic and $n = 471$ cell pairs in wild type). (**B**) Cell-pair distance (x axis) versus correlation coefficient (y axis). Data were fit to a mono-exponential decay curve. In transgenic mice (red), cell pairs exhibited significantly correlated activity at distances up to 200 μm ($P < 0.01$, Kruskal-Wallis with Tukey-Kramer post hoc test), whereas in wild-type mice (blue) cell pairs were not correlated at intercellular distances greater than 50 μm ($P = 0.65$, Kruskal-Wallis with Tukey-Kramer post hoc test).

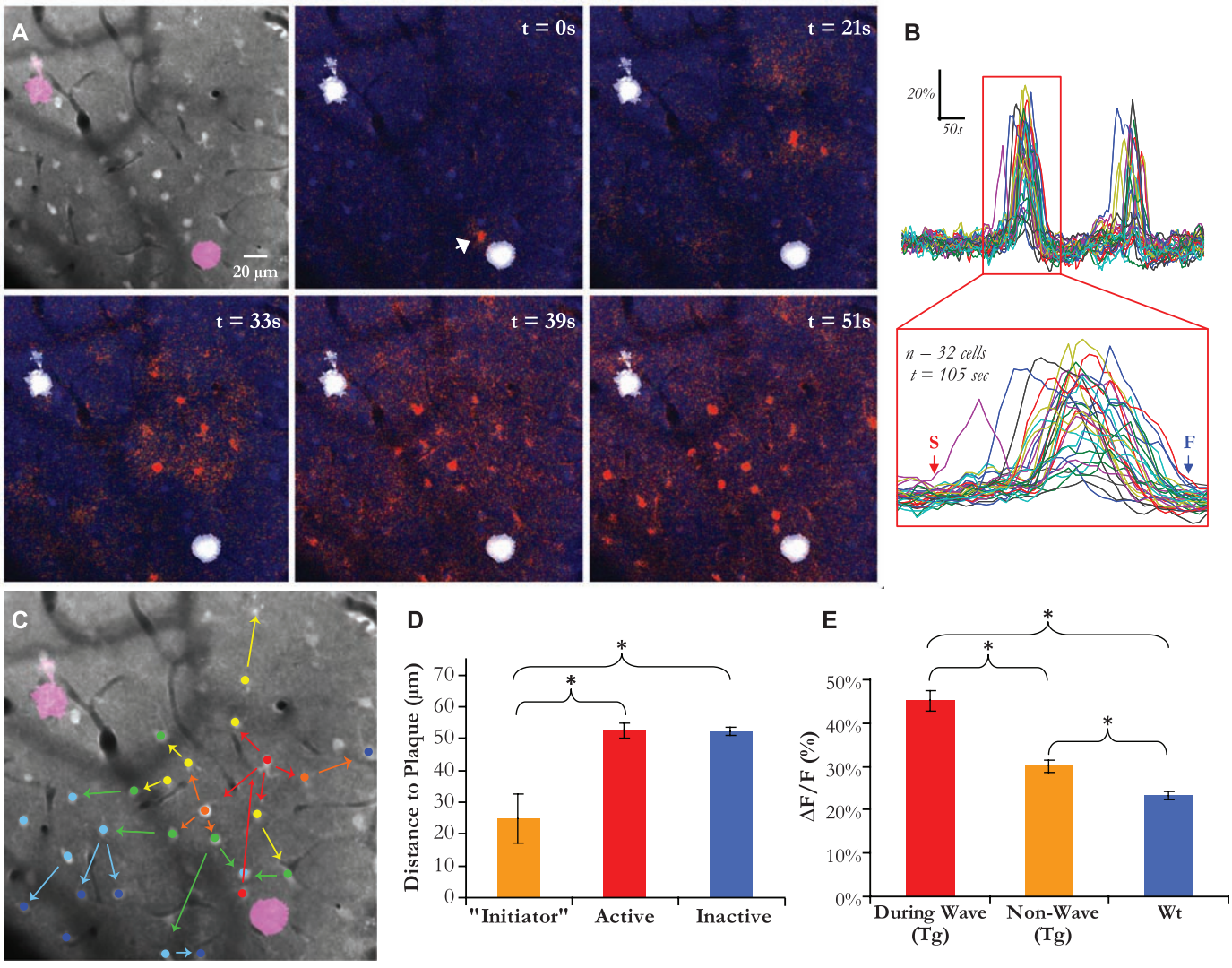

Fig. 4. ICWs in mice with cortical plaques. (**A**) A time-lapse $\Delta F/F$ image filmstrip and (**B**) cell-resolved time course of calcium activity in an APP/PS1 transgenic mouse. The white arrow in the second panel points to the initiator astrocyte, and the sequential panels show the propagation of the wave. (**C**) A summary of (A) in which color denotes temporal sequence and arrows denote spatial propagation. (**D**) Astrocytes that initiate ICWs were closer to senile plaques than the average active or inactive astrocyte (*$P < 0.05$, Kruskal-Wallis with Tukey-Kramer post hoc test). (**E**) There was a significant increase in the amplitude of the calcium signal during a wave [*$P < 0.001$, analysis of variance with Tukey-Kramer post hoc test, $n = 47$ cells in transgenic mice (wave), $n = 156$ cells in transgenic mice (nonwave), $n = 168$ in wild-type mice].

In the AD model, astrocytes exhibited network-wide elevations in resting calcium and increased network-level functional activity. Thus, it appears that astrocytes may represent functionally adaptive cells that play distinct roles in health versus disease. The astrocytic network amplified the effects of focal amyloid deposition across a larger cortical network landscape, perhaps contributing to the global alterations in cortical function and possibly the memory disorders seen in AD. One mechanism underlining this amplification effect is the propagation of ICWs. The observed ICWs typically began in the local plaque microenvironment, suggesting that plaques or plaque-associated bioactive species might induce these powerful calcium waves that travel across the cortex. Since the initial discovery of ICWs nearly two decades ago (*17*), their existence in culture and in acute slices has never been confirmed in vivo (*16*, *18*). Their propagation, through gap junctions (*19*) or via adenosine 5′-triphosphate (*20*, *21*), has been postulated to signal the existence of a pathological insult (*16*, *18*). Our data support this hypothesis because plaque deposition has been linked extensively to neuronal trauma (*1*, *4*, *22*).

The increased astrocyte activity cannot be explained by a simple coupling mechanism with neuronal activity. First, neuronal calcium homeostasis is most severely impaired near senile plaques (*4*), whereas here resting calcium was globally elevated in astrocytes. Second, neurons exhibit a pronounced hyperactivity near plaques (*2*), whereas here astrocytes were more active both near and far from plaques. Third, abolishing neuronal activity had no measurable effect on astrocytic calcium oscillations. Thus, whereas senile plaque deposition induces local synapto- and neurotoxicity, the same Aβ deposits might catalyze astrocytic intra- and intercellular signaling events. This idea is supported in part by evidence that cultured astrocytes exhibit elevated calcium upon application of Aβ but are surprisingly resistant to cell death (unlike neurons) (*23*). An important question that remains unanswered is whether modulating astrocytic calcium signaling, via genetic (*24*) or pharmacological manipulations, will result in dynamic changes in amyloid accumulation (*10*) or alter neuronal network activity associated with behavioral impairments.

References and Notes

1. M. Meyer-Luehmann *et al.*, *Nature* **451**, 720 (2008).
2. M. A. Busche *et al.*, *Science* **321**, 1686 (2008).
3. T. L. Spires *et al.*, *J. Neurosci.* **25**, 7278 (2005).

4. K. V. Kuchibhotla *et al.*, *Neuron* **59**, 214 (2008).
5. X. Wang *et al.*, *Nat. Neurosci.* **9**, 816 (2006).
6. J. Schummers, H. Yu, M. Sur, *Science* **320**, 1638 (2008).
7. H. Hirase, L. Qian, P. Bartho, G. Buzsaki, *PLoS Biol.* **2**, E96 (2004).
8. N. J. Maragakis, J. D. Rothstein, *Nat. Clin. Pract. Neurol.* **2**, 679 (2006).
9. J. Wegiel *et al.*, *Neurobiol. Aging* **22**, 49 (2001).
10. T. Wyss-Coray *et al.*, *Nat. Med.* **9**, 453 (2003).
11. T. Takano, X. Han, R. Deane, B. Zlokovic, M. Nedergaard, *Ann. N. Y. Acad. Sci.* **1097**, 40 (2007).
12. C. D. Wilms, H. Schmidt, J. Eilers, *Cell Calcium* **40**, 73 (2006).
13. M. Garcia-Alloza *et al.*, *Neurobiol. Dis.* **24**, 516 (2006).
14. D. R. Borchelt *et al.*, *Neuron* **19**, 939 (1997).
15. C. Agulhon *et al.*, *Neuron* **59**, 932 (2008).
16. E. Scemes, C. Giaume, *Glia* **54**, 716 (2006).
17. A. H. Cornell-Bell, S. M. Finkbeiner, M. S. Cooper, S. J. Smith, *Science* **247**, 470 (1990).
18. T. A. Fiacco, K. D. McCarthy, *Glia* **54**, 676 (2006).
19. S. Boitano, E. R. Dirksen, M. J. Sanderson, *Science* **258**, 292 (1992).
20. M. L. Cotrina, J. H. Lin, J. C. Lopez-Garcia, C. C. Naus, M. Nedergaard, *J. Neurosci.* **20**, 2835 (2000).
21. P. B. Guthrie *et al.*, *J. Neurosci.* **19**, 520 (1999).
22. M. Garcia-Alloza, S. A. Dodwell, M. Meyer-Luehmann, B. T. Hyman, B. J. Bacskai, *J. Neuropathol. Exp. Neurol.* **65**, 1082 (2006).
23. A. Y. Abramov, L. Canevari, M. R. Duchen, *J. Neurosci.* **23**, 5088 (2003).
24. J. Petravicz, T. A. Fiacco, K. D. McCarthy, *J. Neurosci.* **28**, 4967 (2008).
25. We thank K. O. Ohki and R. C. Reid for assistance with the multicell bolus loading technique. This work was supported by NIH grants EB000768 (B.J.B.), AG08487 (B.T.H.), and NS580752 (K.V.K.).

Supporting Online Material

www.sciencemag.org/cgi/content/full/323/5918/1211/DC1
Materials and Methods
Figs. S1 to S6
Movies S1 and S2
References

27 November 2008; accepted 16 January 2009
10.1126/science.1169096

Meropenem-Clavulanate Is Effective Against Extensively Drug-Resistant *Mycobacterium tuberculosis*

Jean-Emmanuel Hugonnet,[1] Lee W. Tremblay,[1] Helena I. Boshoff,[2] Clifton E. Barry 3rd,[2] John S. Blanchard[1]*

β-lactam antibiotics are ineffective against *Mycobacterium tuberculosis*, being rapidly hydrolyzed by the chromosomally encoded *blaC* gene product. The carbapenem class of β-lactams are very poor substrates for BlaC, allowing us to determine the three-dimensional structure of the covalent BlaC-meropenem covalent complex at 1.8 angstrom resolution. When meropenem was combined with the β-lactamase inhibitor clavulanate, potent activity against laboratory strains of *M. tuberculosis* was observed [minimum inhibitory concentration ($MIC_{meropenem}$) less than 1 microgram per milliliter], and sterilization of aerobically grown cultures was observed within 14 days. In addition, this combination exhibited inhibitory activity against anaerobically grown cultures that mimic the "persistent" state and inhibited the growth of 13 extensively drug-resistant strains of *M. tuberculosis* at the same levels seen for drug-susceptible strains. Meropenem and clavulanate are Food and Drug Administration–approved drugs and could potentially be used to treat patients with currently untreatable disease.

Tuberculosis is perhaps the most persistent human disease caused by an infectious bacterium, *Mycobacterium tuberculosis*. The death toll remains extremely high, despite the introduction of modern multidrug chemotherapy in the 1960s, with between 1.6 and 2 million fatalities annually. An increasing percentage of human clinical isolates are drug-resistant or multidrug-resistant strains that threaten the ability to treat the disease (*1*). The continued use of multidrug therapy has caused an even more dire problem: strains of *M. tuberculosis* resistant to all first-, second-, and third-line agents. In a recent study from South Africa, 54 of 54 patients infected with such highly resistant strains died with a mean survival time from diagnosis of 16 days (*2*).

Since the discovery of penicillin in 1929 (*3*), the β-lactam class of antibiotics has included some of the most clinically important antibacterial agents. The development of broad-spectrum derivatives of penicillin, such as the cephalosporins and olivanic acid (*4*), coupled with their low inherent toxicity have made them the drugs of choice for the treatment of both Gram-negative and Gram-positive bacterial infections. This class, however, has never provided a compound useful in the treatment of tuberculosis, and β-lactams are only rarely used in the treatment of this disease. One important reason for the lack of efficacy was found in the genome sequence of *M. tuberculosis*, which contains a single, highly active, chromosomally encoded class A (Ambler) β-lactamase (*5*). Recently a genetic knockout of the *blaC*-encoded β-lactamase showed that strains lacking this enzyme were more sensitive to β-lactams (*6*). This suggested that the chemical recapitulation of the genetic knockout could similarly resensitize the organism to existing β-lactam antibiotics.

We recently cloned and expressed the *M. tuberculosis blaC* gene and reported a detailed enzymatic characterization (*7*). BlaC exhibits an exceptionally broad substrate specificity, hydrolyzing penicillins at nearly the diffusion-limited rate, all classes of cephalosporins, and, unexpectedly for a class A extended-spectrum β-lactamase, imipenem and meropenem, both carbapenems. Equally unexpected, the enzyme was only transiently inhibited by the β-lactamase inhibitors sulbactam and tazobactam, penicillanic acid sulfones with potent inhibitory activity against other class A β-lactamases. However, clavulanic acid is the only Food and Drug Administration (FDA)–approved β-lactamase inhibitor that irreversibly inhibits BlaC, suggesting that clavulanic acid may recapitulate the genetic knockout, rendering *M. tuberculosis* susceptible to β-lactam antibiotics.

We have previously shown that meropenem was an extremely slow substrate for *M. tuberculosis* BlaC, being hydrolyzed five orders of magnitude slower than ampicillin. A more detailed investigation of the kinetics of meropenem hydrolysis under near stoichiometric enzyme concentrations revealed a steady-state burst with a magnitude dependent on the concentration of BlaC (Fig. 1A). The reaction of meropenem with the enzyme to form the acyl-enzyme intermediate (acylation half-reaction) is fast relative to hydrolysis of the substrate (deacylation). Extrapolation of the final, linear rate to zero time revealed that enzyme acylation was stoichiometric with meropenem. At a single catalytic enzyme concentration, the linear rates yielded plots typical of Michaelis-Menten kinetics (Fig. 1B), with Michaelis constant $K_m = 3.4 \pm 0.7$ μM and turnover number $k_{cat} = 0.08 \pm 0.01$ min^{-1}. Because of its extremely slow turnover rate, we investigated the possibility that meropenem could act as an inhibitor of BlaC and whether it was possible to trap the covalently acylated form of the enzyme. Meropenem acts as a slow, tight-binding inhibitor of the hydrolysis of the chromogenic β-lactam nitrocefin by BlaC. The time courses of nitrocefin hydrolysis are nonlinear in the presence of meropenem, and an analysis of these data yielded an inhibition constant (K_i) value of 16 ± 2 μM and a K_i* value of 1.1 ± 0.8 μM (fig. S1, A and B). The ability of meropenem to act as an inhibitor of BlaC in addition to being a very poor substrate for BlaC added to its potential as an active partner with clavulanate.

The rapid acylation and slow deacylation of BlaC by meropenem suggested that we could observe the covalently bound species by Fourier transform ion cyclotron resonance (FTICR) mass spectrometry. A freshly prepared solution of

[1]Department of Biochemistry, Albert Einstein College of Medicine, 1300 Morris Park Avenue, Bronx, NY 10461, USA. [2]Tuberculosis Research Section, Laboratory of Clinical Infectious Diseases, National Institute of Allergy and Infectious Diseases, National Institutes of Health, Bethesda, MD 20892, USA.

*To whom correspondence should be addressed. E-mail: blanchar@aecom.yu.edu